# Interannual Variability of the Kuroshio Extension System and Its Impact on the Wintertime SST Field

BO QIU

*Department of Oceanography, University of Hawaii at Manoa, Honolulu, Hawaii*

28 June 1999 and 10 January 2000

ABSTRACT

Altimetry data from the first 7-yr TOPEX/Poseidon (T/P) mission (October 1992–September 1999) are analyzed to investigate the interannual variability in regions of the Kuroshio Extension and its southern recirculation gyre. Large-scale, interannual changes of the Kuroshio Extension system are characterized by the oscillation between an elongated state and a contracted state. In the elongated state, the Kuroshio Extension has a larger eastward surface transport, a greater zonal penetration, and a more northerly zonal-mean path. All these characteristics are closely connected to the presence of an intense, zonally elongated southern recirculation gyre. In its contracted state, the Kuroshio Extension has a smaller eastward surface transport, a more southerly mean path, and is accompanied by a weaker southern recirculation gyre. During the T/P period, the Kuroshio Extension changed from the elongated state in 1992–93 to the contracted state in 1996–97, and back to the elongated state since late 1997.

In addition to these large-scale changes, the mesoscale eddy field also exhibited prominent interannual changes in the Kuroshio Extension region. In the upstream region between the Izu Ridge and the Shatsky Rise, the eddy kinetic energy level was generally low while the Kuroshio Extension was in its elongated state, and high while in the contracted state. Downstream of the Shatsky Rise, on the other hand, the EKE level was high (low) when the Kuroshio Extension was in the elongated (contracted) state. The large-scale, interannual changes in the Kuroshio Extension system have a significant impact on the regional wintertime SST anomaly field: the warm (cold) wintertime SST anomalies tend to persist in years when the Kuroshio Extension is in its elongated (contracted) state. A diagnostic analysis of the surface ocean heat balance indicates that the nonseasonal geostrophic advection by the ocean circulation works to reduce (increase) the wintertime SST anomalies when the Kuroshio Extension changes from an elongated (contracted) state to a contracted (elongated) state. The SST anomalies associated with the large-scale changes of the Kuroshio Extension have an area-averaged, peak-to-peak amplitude of $>1$°C and appear independent of the interannual SST changes in the tropical Pacific Ocean.

## 1. Introduction

After separating from the Japan coast at 35°N, 140°E the Kuroshio enters the open basin of the North Pacific where it is renamed the Kuroshio Extension. Free from the constraint of coastal boundaries, the Kuroshio Extension has been observed to be an eastward-flowing inertial jet accompanied by large-amplitude meanders and energetic pinched-off eddies (e.g., Kawai 1972; Yasuda et al. 1992). Due to its abundance of mesoscale eddy variability, it was recognized more than two decades ago that the Kuroshio Extension region has the highest eddy kinetic energy level in the Pacific Ocean (Wyrtki et al. 1976). The launch of the TOPEX/Poseidon (T/P) satellite in 1992 and its successful multiyear measurements of the sea surface height (SSH) field allow us now not only to improve mapping of the geographical distribution of the oceanic eddy field, but also to examine the interannual changes in high-eddy-variability regions such as the Kuroshio Extension.

Interannual changes in the Kuroshio Extension have been the focus of several previous studies. By analyzing hydrographic and XBT data in the Kuroshio Extension region from 1976 to 1980, Mizuno and White (1983) showed that the Kuroshio Extension was displaced southward, from 36°–37°N during 1977–78 to 34°N in 1979–80. Associated with this large-scale path change, the quasi-stationary meander pattern of the Kuroshio Extension became unstable and eddy activity and the ring formation rate increased. Using available temperature measurements from 1950 to 1970, Yamagata et al. (1985) showed that on interannual time scales, the baroclinic transport of the Kuroshio Extension had a lagged, positive correlation with that of the upstream North Equatorial Current (NEC). Following individual ENSO events when the NEC transport increased, the Kuroshio Extension tended to intensify 1.5 years later.

*Corresponding author address:* Dr. Bo Qiu, Department of Oceanography, University of Hawaii at Manoa, 1000 Pope Road, Honolulu, HI 96822.
E-mail: bo@soest.hawaii.edu

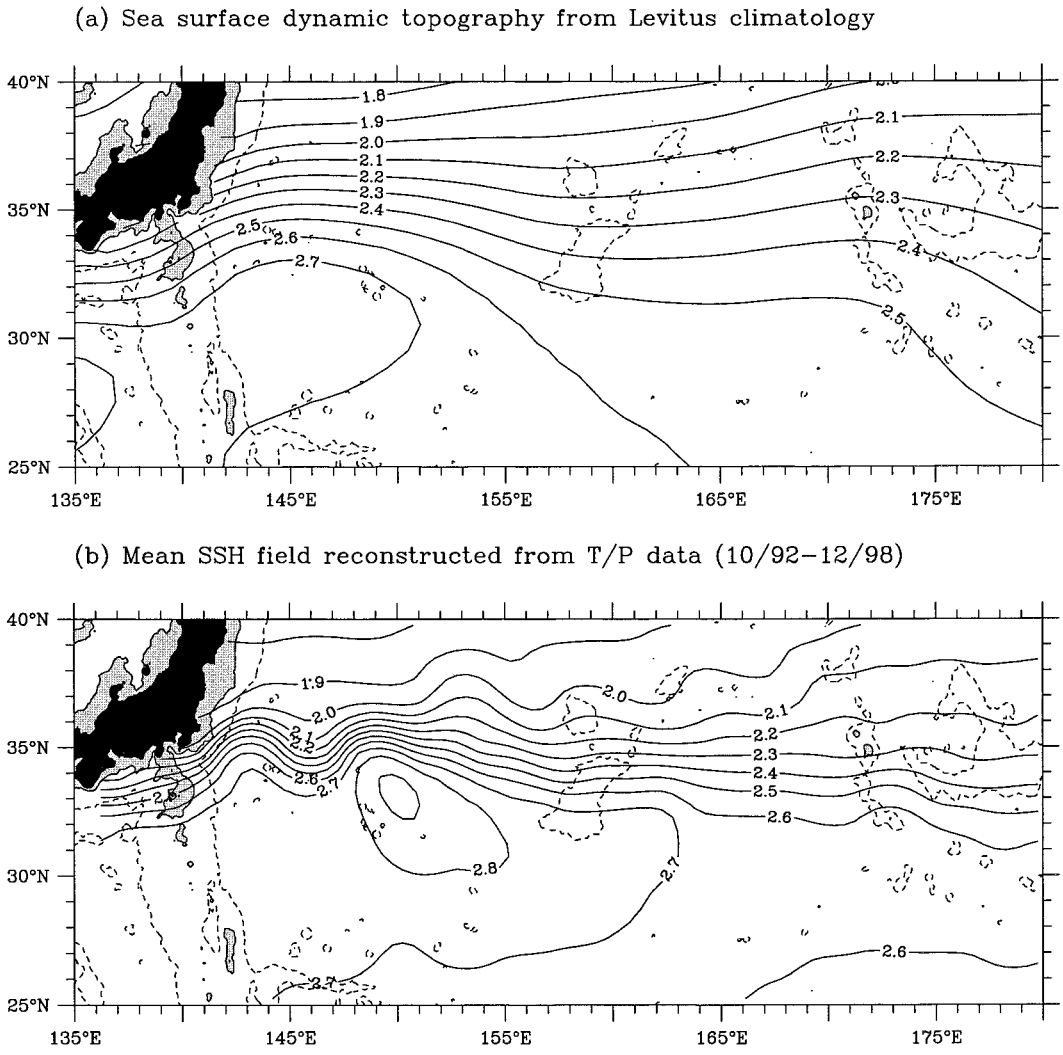


FIG. 1. (a) Sea surface topography (in meters) relative to 2000 dbar calculated from the Levitus (1982) climatology. (b) Mean SSH field reconstructed from the T/P data (Oct 1992–Dec 1998). Dashed lines denote the 4000-m isobaths, and areas shallower than 1000 m are shaded. Major bathymetric features here include the Izu–Ogasawara Ridge along 141°E, the Shatsky Rise near 159°E, and the Emperor Seamounts along 172°E.

With the advent of satellite altimetry, several investigators have examined the interannual changes of the Kuroshio Extension using altimetrically derived SSH data. Based on the data from the Geosat Exact Repeat Mission, Qiu et al. (1991) showed that the changes in the zonal-mean surface transport of the Kuroshio Extension were significantly correlated to the changes in the zonal-mean position of the Kuroshio Extension. Over the 2.5-yr Geosat period from November 1986 to April 1989, the Kuroshio Extension had a steady increase in its surface transport and a concurrent northward migration in its mean path. This interannual trend in transport and path of the Kuroshio Extension was found reversed during the first 2-yr T/P period. Qiu (1995) attributed the decline in the Kuroshio Extension's surface transport and its concurrent southward path migration in 1992–94 to the weakening of the Kuroshio Extension's southern recirculation gyre. By examining the linear SSH trend over a 4-yr period of the T/P mission, Wang et al. (1998) found that this decline in the eastward flowing Kuroshio Extension and its associated recirculation gyre was not confined to 1992–94, but continued into late 1996. Also using the T/P SSH data, Adamec (1998) found a significant interannual modulation in the seasonal eddy kinetic energy (EKE) field along the path of the Kuroshio Extension. By combining the SSH data with advanced very high-resolution radiometer SST data, Adamec showed that these observed EKE changes were not a result of regional wind and/or buoyancy forcings, but due to the ocean's internal adjustment through convergence of eddy heat fluxes.

One objective of this study is to extend the examination of the interannual changes in the Kuroshio Extension and its recirculation gyre system. Indeed, the

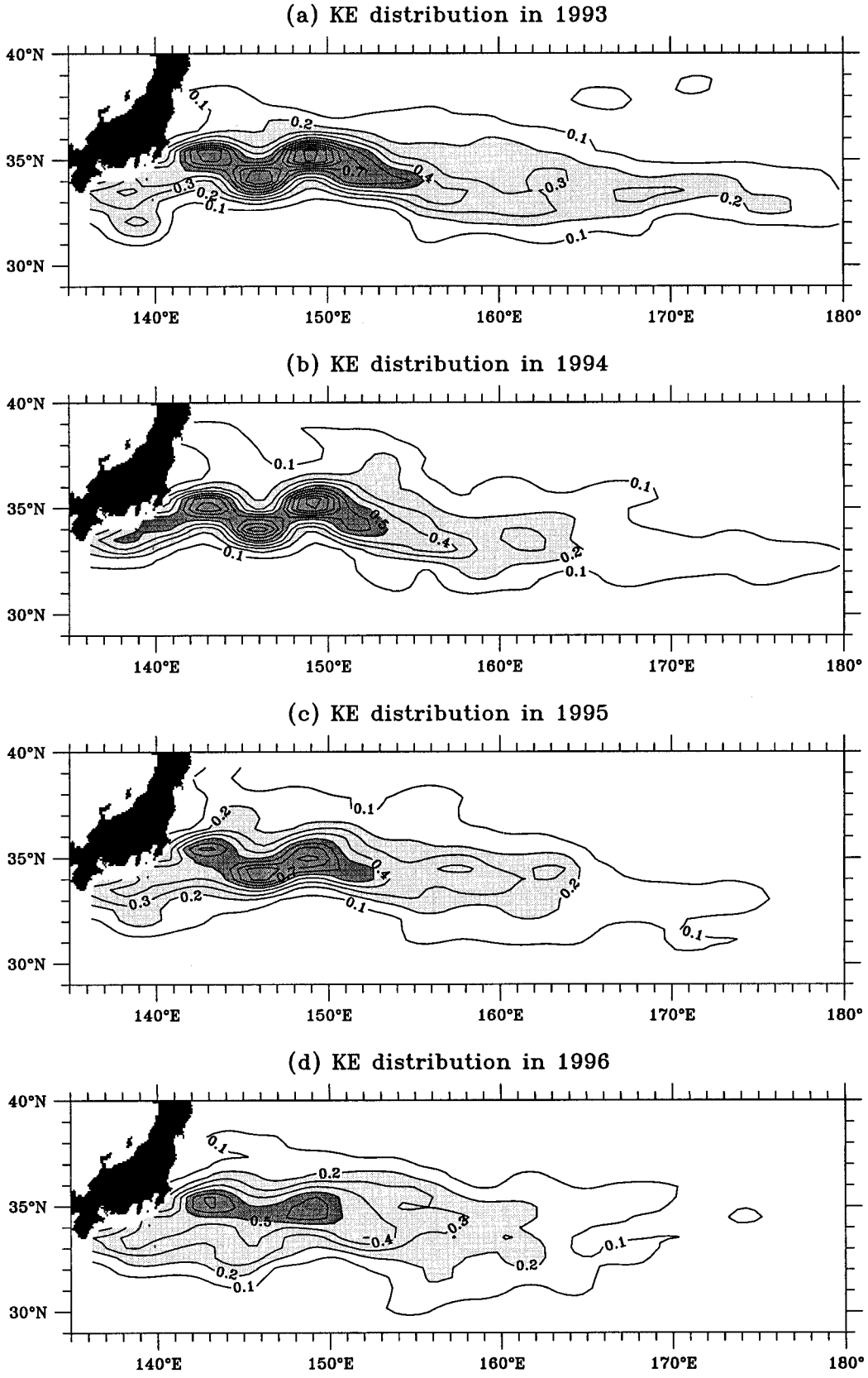
(a) KE distribution in 1993
(b) KE distribution in 1994
(c) KE distribution in 1995
(d) KE distribution in 1996
40°N
35°N
30°N
140°E
150°E
160°E
170°E
180°

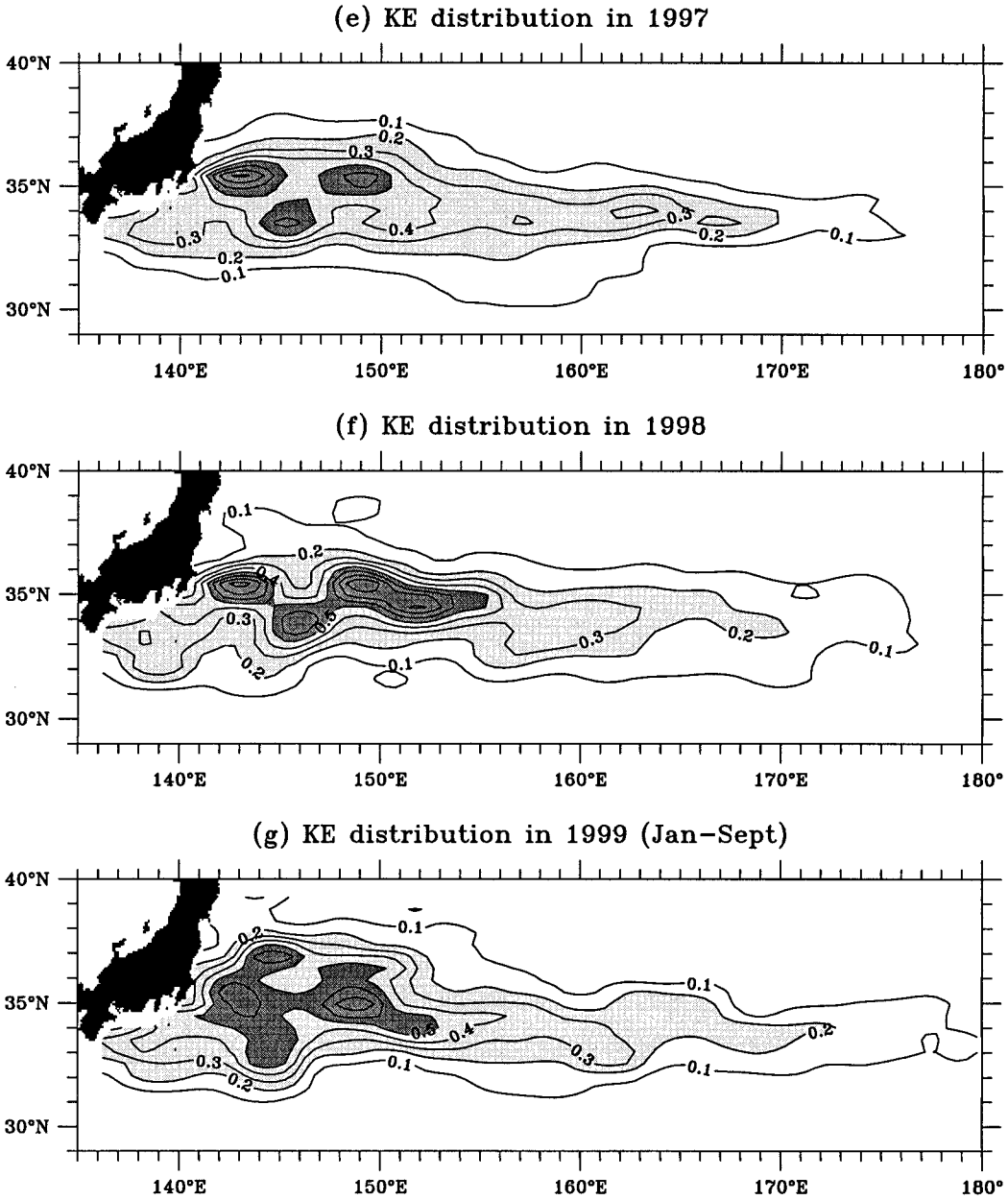


FIG. 2. (*Continued*)

interannual trend in the Kuroshio Extension's transport/path after 1996 became opposite to that detected during the earlier years of the T/P mission. Accompanying these interannual changes in the large-scale Kuroshio Extension system, mesoscale eddy activity also underwent significant interannual modulations. In this study, we will contrast the interannual changes in the mesoscale eddy field with the large-scale transport/path changes of the Kuroshio Extension.

In addition to describing the Kuroshio Extension's changes on the interannual timescales, this study will further assess how these changes may affect regional wintertime sea surface temperature (SST) distributions. The largest heat loss from the ocean to atmosphere over

←

FIG. 2. Yearly averaged kinetic energy distributions estimated from the along-track absolute SSH data. Contour intervals are 0.1 $m^2 s^{-2}$. Light-shaded areas indicate energy levels greater than 0.2 $m^2 s^{-2}$ and dark-shaded areas indicate energy levels greater than 0.5 $m^2 s^{-2}$.

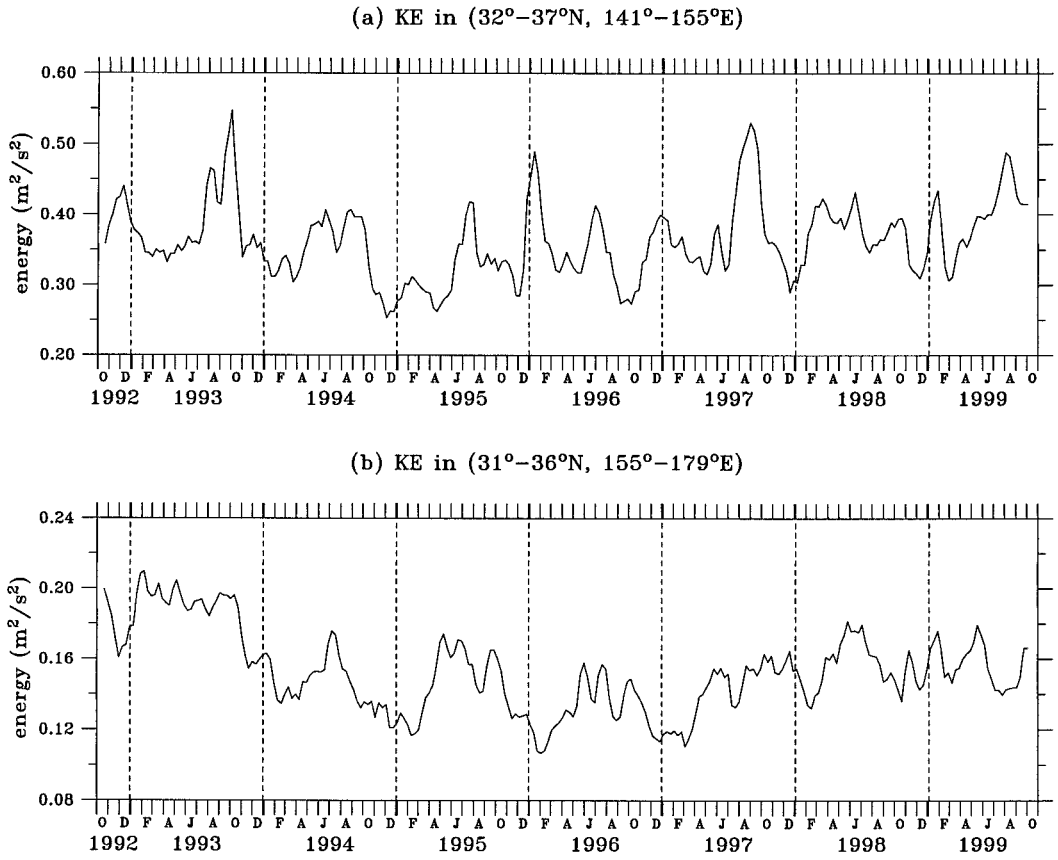


FIG. 3. Time series of the kinetic energy averaged in (a) the upstream Kuroshio Extension region (32°–37°N, 141°–155°E) and (b) the downstream Kuroshio Extension region (31°–36°N, 155°–179°E).

the North Pacific Ocean occurs in the Kuroshio Extension region. This large heat loss, with the maximum net heat flux value exceeding 450 W $m^{-2}$ (da Silva et al. 1994), is due in part to the contact of cold, continental air with the warm water transported poleward by the Kuroshio. As the area of the maximum air–sea heat exchange is located where the oceanic variability is also at a maximum, it is conceivable that the large-scale fluctuations occurring in the Kuroshio Extension system could alter the upper ocean heat budget, thereby modifying the SST distributions. On the interannual-to-decadal timescales, persistent SST anomalies in the Kuroshio Extension region can influence the overlying atmospheric circulation over the midlatitude North Pacific Ocean (e.g., Peng et al. 1997; Barnett et al. 1999), whose change in turn can affect the basin-scale oceanic circulation through surface wind stress forcing. This ocean–atmosphere coupling through the SST anomalies in the western boundary current outflow region has been proposed by Latif and Barnett (1994, 1996) to be essential for generating the Pacific decadal oscillation.

Recent studies by Miller et al. (1998), Deser et al. (1999), and Xie et al. (2000) provided clear evidence that the decadal changes in the strength of the Kuroshio Extension can have a strong impact on the subsurface temperature structures of the Kuroshio Extension region. How the low-frequency changes of the Kuroshio Extension can affect the SST field is more complicated, because the SST is affected also by other processes, such as surface heat flux forcing, surface Ekman advection, and entrainment/detrainment associated with the evolution of the mixed layer. Although anomalous surface heat flux forcing has been considered to be the dominant contributor to nonseasonal SST anomalies in the midlatitudes, Cayan (1992) and Iwasaka and Wallace (1995) found that the time-rate-of-change of SST anomalies and the anomalous surface heat flux are not as highly correlated in the Kuroshio Extension region as they are in the regions over the central and eastern North Pacific. In contrast to 0.6 in the latter regions, a typical correlation coefficient in the Kuroshio Extension region is about 0.4 (see, e.g., Iwasaka and Wallace's Fig. 6). This result hints at the importance of the regional ocean dynamics in influencing the nonseasonal SST changes. Using the surface ocean circulation information from the T/P data and by carrying out an upper-ocean heat budget analysis, we will show that a significant part of the observed nonseasonal SST signals are related to the interannual changes of the Kuroshio Extension system.

Following a brief description of the T/P SSH data

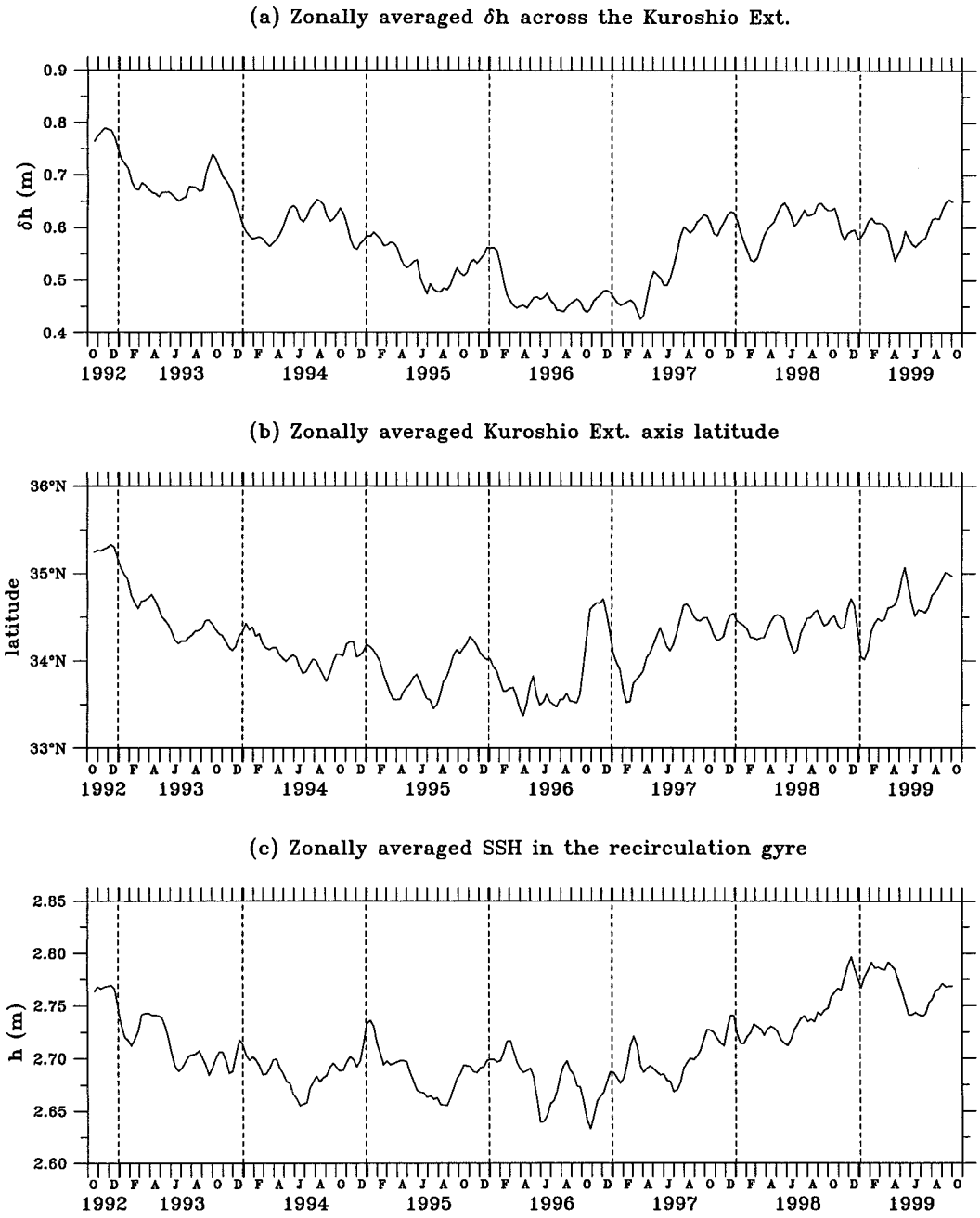


FIG. 4. Time series of (a) the zonally averaged SSH difference across the Kuroshio Extension, (b) the zonally averaged axis position of the Kuroshio Extension, and (c) the zonally averaged SSH in the recirculation gyre. Here, the zonal average is from 141°E to 180°.

and the mean SSH field in the next section, we will describe in section 3 the interannual changes in the kinetic energy field of the Kuroshio Extension. In section 3, we will also examine the Kuroshio Extension's transport/path fluctuations and their connection to the changes in the southern recirculation gyre. The impact of the interannual variability of the Kuroshio Extension on the nonseasonal wintertime SST changes is assessed in section 4. Section 5 summarizes the results from this study.

## 2. SSH data: Anomalies and the mean field

The first seven years of the T/P altimeter data, from October 1992 through September 1999 (cycles 2 to 258), are used in this study. To focus on the Kuroshio Extension and its southern recirculation gyre, we processed all 36 ascending and descending tracks in the domain of 25°–40°N lat, 136°E–180° long. In a western boundary current outflow region such as the Kuroshio Exten-

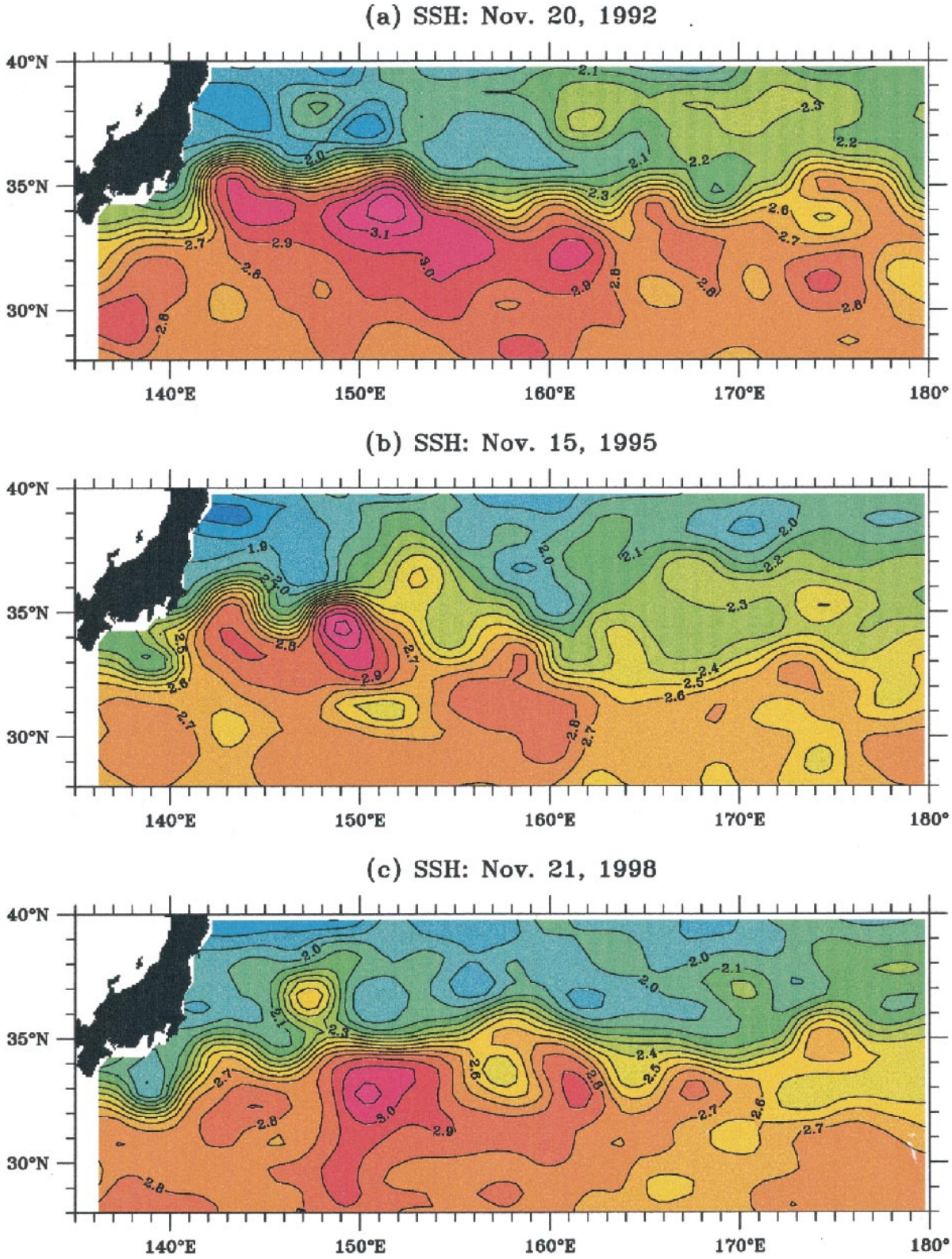


FIG. 5. Sea surface height fields on (a) 20 Nov 1992, (b) 15 Nov 1995, and (c) 21 Nov 1998.

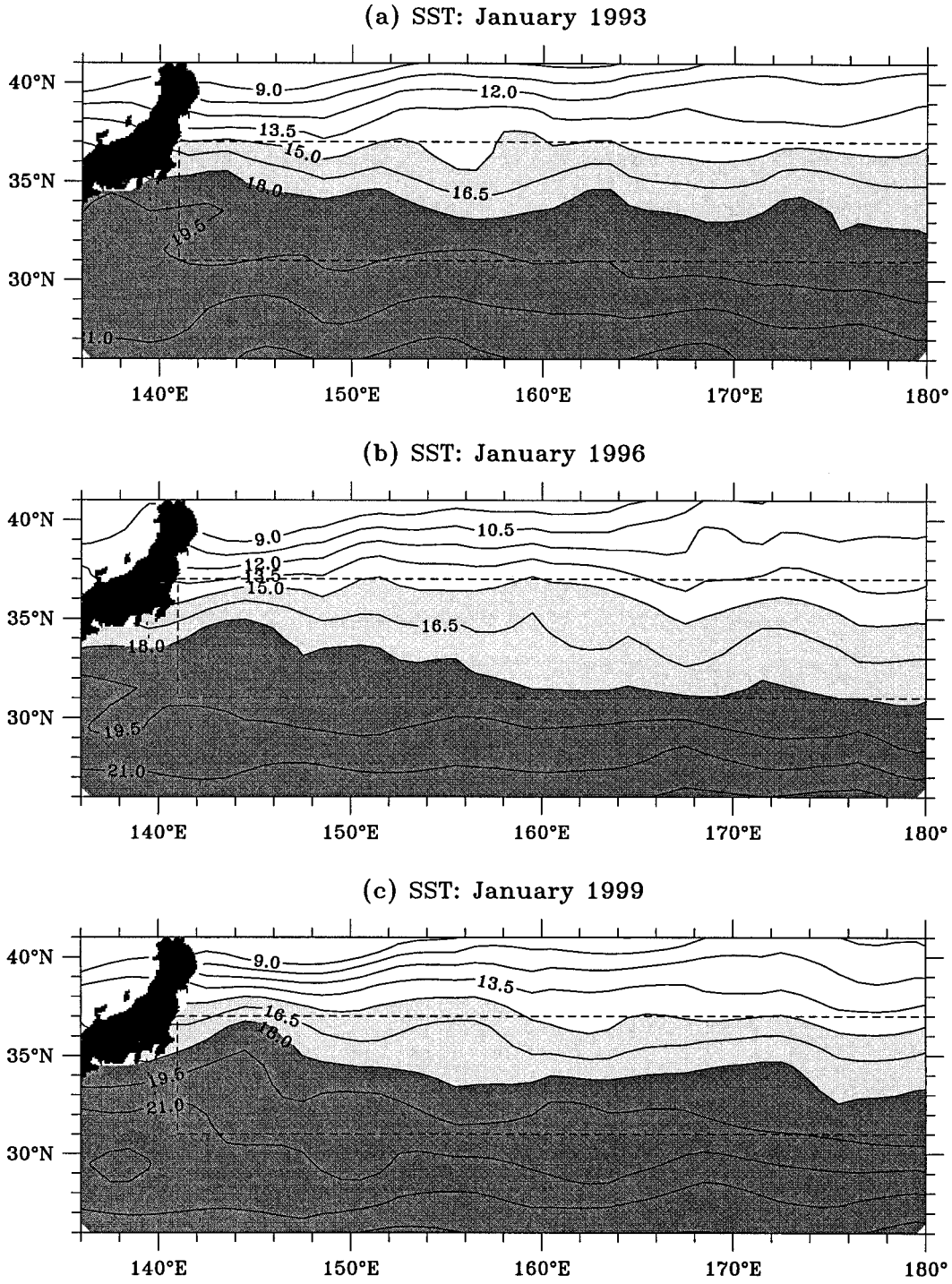


FIG. 6. Sea surface temperature fields in January of (a) 1993, (b) 1996, and (c) 1999 from the 1°-gridded SST dataset of NCEP. Light-shaded areas indicate 15°C < SST < 18°C and dark-shaded areas indicate SST > 18°C. The dashed box denotes the Kuroshio Extension region.

sion, a significant part of the altimetrically measured SSH signals is due to the seasonally varying surface buoyancy fluxes, which cause expansion or contraction of the water column (Wang and Koblinsky 1996; Stammer 1997; Vivier et al. 1999). These so-called steric height signals have spatial scales much greater than those of oceanic mesoscale eddies and their effect is largely confined to the seasonal thermocline of the upper ocean (Gill and Niiler 1973). As the steric height signals are not the focus of this study, they are removed from

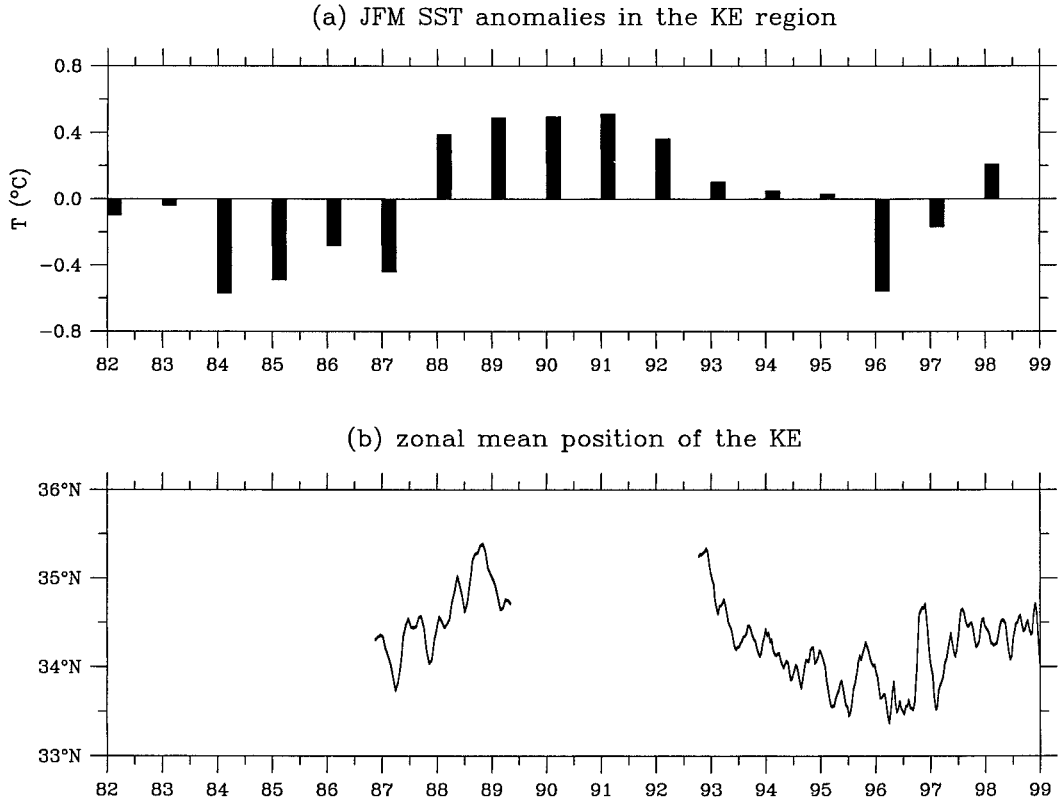


FIG. 7. (a) Time series of the wintertime SST anomalies averaged in the Kuroshio Extension region (31°–37°N, 141°E–180°). (b) Time series of the mean axis position of of the Kuroshio Extension from 141°E to 180°. The axis data are from both the Geosat ERM period of late 1980s and the recent T/P period.

the alongtrack SSH anomaly data in our following analysis. To remove the steric height signals, we followed the procedures described in Stammer (1997) and used the daily net surface heat flux data for the T/P period from the National Centers for Environmental Prediction (NCEP).

Note that the steric height signal represents that part of the SSH signals *directly* induced by the surface buoyancy fluxes. The surface buoyancy forcing in the western boundary current outflow region can also influence the SSH field *indirectly* through strengthening of the recirculation gyre (e.g., Huang 1990) and through subduction of the wintertime mixed layer water into the main thermocline. Removal of the steric height signals has little impact upon the SSH signals that are indirectly induced by the surface buoyancy fluxes.

To better describe the variability of the Kuroshio Extension system, information about the mean SSH field, which is not readily available from altimetric measurements due to the uncertainty in the geoid, is desirable. For the Kuroshio Extension, a useful method for reconstructing the alongtrack mean SSH profile is to use a kinematic jet model that fits the altimetric SSH data to a shape function representing the eastward-flowing surface jet (Kelly and Gille 1990; Qiu et al. 1991). Qiu (1995) described in detail how the kinematic jet model can be extended to include the westward recirculating flows of the Kuroshio Extension. The net surface transport of the Kuroshio Extension system (namely, the eastward jet plus the westward recirculating flows) in this case is constrained by the climatological surface dynamic height field of Levitus (1982; Fig. 1a). Following the procedures described in Qiu (1995), we reconstructed the along track mean SSH profiles with the use of the T/P data of 1992 to 1998. Figure 1b shows the mean SSH field objectively mapped from the along-track mean SSH profiles. For a discussion on features of the mean Kuroshio Extension (such as, the presence of the quasi-stationary meanders and the southern recirculation gyre), readers are referred to Qiu (1995). Once the mean SSH field $\overline{h}$ is estimated, the absolute SSH field is simply the sum of the mean field and the time-varying anomaly field: $h = \overline{h} + h'$.

## 3. Interannual changes in the Kuroshio Extension system

Using the 7-yr time series of the T/P SSH data, we examine first the interannual changes in the kinetic energy (KE) field of the Kuroshio Extension region. Figure 2 shows the yearly averaged KE distributions from 1993 to 1999. Here, KE is estimated from the alongtrack SSH

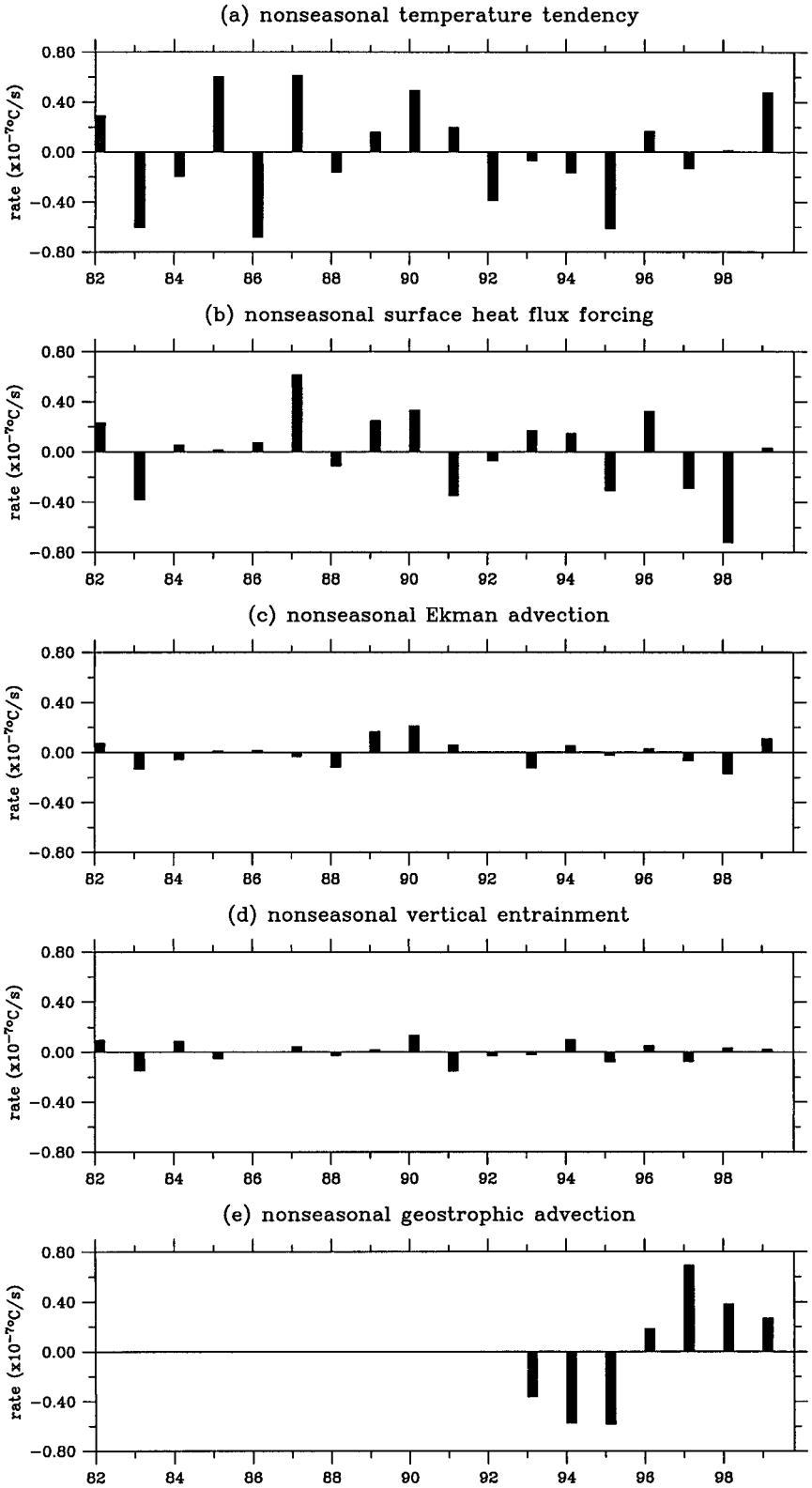


FIG. 8. Time series of the nonseasonal values for the five terms in Eq. (2). The J/F/M mean values for each term are listed in Table 1.

TABLE 1. Mean wintertime (J/F/M) balance for the mixed layer temperature equation [Eq (2)]. Values are averaged in the Kuroshio Extension region of 31°–37°N, 141°E–180°. Units in $10^{-7}$ °C $s^{-1}$.

| | 1982–99 | 1993–99 |
|---|---|---|
| $\overline{\partial T_m/\partial t}$ | −2.63 | −2.67 |
| $\overline{Q_{net}/\rho_o c_p h_m}$ | −2.85 | −2.94 |
| $\overline{-\mathbf{u}_e\cdot\nabla T_m}$ | −0.45 | −0.48 |
| $\overline{-w_e(T_m-T_d)/h_m}$ | −0.59 | −0.59 |
| $\overline{-\mathbf{u}_g\cdot\nabla T_m}$ | | +1.52 |
| Residual | −1.26 | +0.18 |

TABLE 2. Linear correlation coefficient between the nonseasonal temperature tendency term and the terms (their nonseasonal time series) on the rhs of Eq. (2). Here, hf denotes the surface heat flux forcing term, Ea the Ekman advection term, ve the vertical entrainment term, and ga the geostrophic advection term.

| | 1982–99 | 1993–99 |
|---|---|---|
| $\left(\frac{\partial T_m}{\partial t}\right)'$ vs (hf)′ | 0.47 | 0.30 |
| $\left(\frac{\partial T_m}{\partial t}\right)'$ vs (hf + Ea)′ | 0.51 | 0.34 |
| $\left(\frac{\partial T_m}{\partial t}\right)'$ vs (hf + Ea + ve)′ | 0.52 | 0.38 |
| $\left(\frac{\partial T_m}{\partial t}\right)'$ vs (hf + Ea + ve + ga)′ | | 0.80 |

data ($h$) by assuming geostrophy and the isotropic condition, namely,

$$\text{KE} \equiv \langle u_g^2 \rangle \quad \text{with } u_g = -\frac{g}{f}\frac{\partial h}{\partial s}, \tag{1}$$

where $f$ is the Coliolis parameter, $s$ is the alongtrack distance, and angle brackets denote the ensemble average from both the ascending and descending track estimates. Note that although the isotropic condition was shown to be a good assumption for the time-varying surface flow of the Kuroshio Extension along 152°E by Schmitz (1984) and Hall (1989), its validity over the wider region of the Kuroshio Extension system and over various timescales needs to be proved in future studies.

Year-to-year changes in the kinetic energy field of the Kuroshio Extension region are substantial. Figure 2a shows that the high KE area in 1993 was confined in latitude with its center following closely the mean path of the Kuroshio Extension (cf. Fig. 1b). Three KE maxima existed in the upstream region and corresponded to the ridges and the trough of the two quasi-stationary meanders of the Kuroshio Extension, respectively. In Fig. 2a, the high KE band defined, say, by the 0.2 $m^2$ $s^{-2}$ contour extends beyond 175°E. The zonal extent of this high KE band was reduced significantly in 1994; the 0.2 $m^2$ $s^{-2}$ contour in Fig. 2b reached only to 165°E. A further decrease in size of the high KE area is seen in 1995, in which the 0.1 $m^2$ $s^{-2}$ contour retreated westward to 176°E (Fig. 2c). In the upstream region in 1995, there was a decrease in the kinetic energy level associated with the quasi-stationary meanders of the Kuroshio Extension as well.

The zonal penetration of the high KE band was at its minimum in 1996 (Fig. 2d). In this year, while the maximum kinetic energy level dropped further in the upstream Kuroshio Extension region, the high KE band itself showed a sizable expansion in the meridional direction. This widening of the high KE band continued in 1997 in the upstream Kuroshio Extension region (Fig. 2e). An examination of sequential SSH maps (not shown here) reveals that the upstream Kuroshio Extension region in 1996/97 was dominated by events in which energetic cold-core eddies detach from the Kuroshio Extension around 155°E, migrate westward, and interact intensely with the main body of the Kuroshio Extension after they encounter the shoaling Izu Ridge near 141°E. The meridionally widened high KE distributions seen in Figs. 2d and 2e are a manifestation of this intense eddy–mean flow interaction. In 1998 and 1999 (Figs. 2f and 2g), the KE field appeared to be returning to its pre-1994 condition with the high KE band expanding gradually in the zonal direction.

Figure 3a shows the time series of the KE averaged in the upstream Kuroshio Extension region (32°–37°N, 141°–155°E). Notice that the area-averaged KE level in 1996/97 is similar to those in 1993 and 1998/99. In other words, on the interannual timescale, the total kinetic energy in the upstream Kuroshio Extension region remained nearly constant regardless of whether the Kuroshio Extension path fluctuated actively in the meridional direction or stayed close to its climatological mean position. In contrast, the area-averaged KE level has a well-defined interannual signal in the downstream Kuroshio Extension region (31°–36°N, 155°–179°E). As shown in Fig. 3b, the KE level was high in 1993 and decreased gradually in the subsequent three years. The decreasing trend reversed after 1997. From the yearly KE maps of Fig. 2, it is obvious that this interannual signal reflects the interannual changes in the zonal penetration of the high KE band.

In addition to the kinetic energy field, interannual changes also appear in other aspects of the Kuroshio Extension system. Figure 4a shows the time series of the zonally averaged SSH difference ($\delta h$) across the eastward-flowing Kuroshio Extension. Here, $\delta h$ is evaluated first along individual T/P tracks by identifying the center of the Kuroshio Extension jet (where the eastward surface flow is maximum), averaging the SSH values over a 1° bin 1.5 degrees north and south of the jet's center ($h_N$ and $h_S$), and taking the difference, $h_S - h_N$. A zonal average is then taken from 141°E to 180° to

remove effects of mesoscale signals. Thus defined, $\delta h$ is proportional to the mean surface transport of the eastward-flowing Kuroshio Extension. The interannual signal of $\delta h$ is similar to that shown in Fig. 3b; that is, it has a decreasing trend from 1993 to 1996 and the trend reverses after 1997. Physically, that these two time series should match on the interannual time scales is of no surprise. The time series of Fig. 3b, as we noted above, is a measure of the zonal penetration of the high KE band. A larger $\delta h$ in Fig. 4a signifies a more intense Kuroshio Extension jet, whose greater zonal penetration is likely to give rise to a higher KE level in the downstream Kuroshio Extension region.

To make this point more explicit, we compare in Fig. 5 the SSH maps for November of 1992, 1995, and 1998. In November 1992 when it had a relatively large surface transport, Fig. 5a shows that the Kuroshio Extension had a coherent zonal-jet structure extending beyond the date line. In contrast, the jetlike structure was no longer obvious near 160°E in November 1995, when $\delta h$ was relatively small (Fig. 5b). As the surface transport restrengthened in 1998, the zonal jet of the Kuroshio Extension was found to reach the date line again (Fig. 5c). Notice that the interannual changes in $\delta h$ are positively correlated with the interannual changes in the zonally averaged position of the Kuroshio Extension jet. As presented in Figs. 4a and 4b, a larger surface transport of the Kuroshio Extension tends to correspond to a more northerly position. This positive correlation between the surface transport and position of the Kuroshio Extension was also found in the Geosat ERM period of November 1986–May 1989 (Qiu et al. 1991), and a similar positive correlation exists in the Gulf Stream system as well (Kelly 1991; Kelly et al. 1999).

The cause for this positive correlation can be sought in the low-frequency variability of the recirculation gyre. In Fig. 4c, we plot the time series of the SSH ($h_R$) averaged in the Kuroshio Extension recirculation gyre region from 141°E to 180° and from 28°N to the southern edge of the Kuroshio Extension jet (defined at 2° south of the jet's center). A high $h_R$ value in Fig. 4c indicates a strong anticyclonic recirculation gyre and vice versa. Given that the transport increase of the Kuroshio Extension compared to the interior Sverdrup transport is due to the presence of the recirculation gyre, we may expect $\delta h$ and $h_R$ be correlated on the interannual timescale. As shown in Figs. 4a and 4c, this indeed is the case. That a more intense Kuroshio Extension is accompanied by a stronger recirculation gyre can also be visually confirmed in Fig. 5: compared with 1995 shown in Fig. 5b, the recirculation gyre in 1992 and 1998 (Figs. 5a and 5c) had a greater zonal and meridional extent. From Figs. 4 and 5, it is clear that the low-frequency changes of the Kuroshio Extension are closely related to those of the recirculation gyre. As the recirculation gyre intensifies, it elongates zonally, increasing the zonal-mean eastward transport of the Kuroshio Extension and shifting its zonal-mean position northward. When the recirculation gyre weakens, it decreases the eastward transport of the Kuroshio Extension and shifts its zonal-mean position southward.

## 4. Impact on the wintertime SST field

As we noted in the introduction, the Kuroshio Extension region is where one finds the strongest air–sea interaction in the extratropical North Pacific. Given the large interannual changes in the Kuroshio Extension's surface transport and path, it is natural to ask to what extent these changes may affect the regional SST distributions. Like in many previous studies (e.g., Miller et al. 1994; Deser and Blackmon 1995; Nakamura et al. 1997), we will in the following focus on the SST signals of wintertime (J/F/M) because this is the season when the air–sea interaction is most active. Figure 6 shows the January SST maps of 1993, 1996, and 1999 compiled by the NCEP's Environmental Modeling Center (Reynolds and Smith 1994). These three SST maps correspond to the three SSH maps in Fig. 5 by a respective 2-month lag. A visual comparison between Figs. 5 and 6 indicates that the SST in the Kuroshio Extension region was colder in January 1996, when the surface transport of the Kuroshio Extension was weak and its zonal-mean path was relatively southerly. In comparison, when the Kuroshio Extension was more intense and its path more northerly in 1992 and 1998, the wintertime SST in the Kuroshio Extension region was warmer.

For a more quantitative comparison, we plot in Fig. 7a the time series of the wintertime SST anomalies averaged in the region of 31°–37°N, 141°E–180°. Here, the SST anomalies are defined as the J/F/M SST deviations from the mean J/F/M SST value of 1982 to 1999. Figure 7a shows a clear interannual-to-decadal signal with cold SST anomalies appearing in 1984–87 and 1996–97 and warm SST anomalies in 1988–92 and 1999. The peak-to-peak amplitude of the interannual SST anomalies exceeds 1°C. Figure 7b shows the time series of the zonal-mean axis position of the Kuroshio Extension; here the time series for the T/P period is the same as in Fig. 4b and the time series for the Geosat ERM period is adapted from Fig. 12 of Qiu et al. (1991). Comparing the two time series in Fig. 7 confirms the general trend we noted above, namely, on the interannual timescales, warm (cold) wintertime SST anomalies in the Kuroshio Extension region tend to coincide with the northerly (southerly) paths of the Kuroshio Extension.

In order to assess quantitatively the effect of the interannual variability of the Kuroshio Extension on the wintertime SST anomaly field, we examine below the heat balance in the surface ocean mixed layer:

$$\frac{\partial T_m}{\partial t} = \frac{Q_{\text{net}}}{\rho_o c_p h_m} - \mathbf{u}_e \cdot \nabla T_m - \frac{w_e(T_m - T_d)}{h_m} - \mathbf{u}_g \cdot \nabla T_m, \quad (2)$$

where $T_m$ denotes the mixed layer temperature and is a good proxy for SST in winter. In Eq. (2), $Q_{\text{net}}$ denotes the net surface heat flux, $\rho_o$ and $c_p$ are the reference density and specific heat of seawater, $h_m$ is the mixed layer depth, $\mathbf{u}_e$ is the Ekman velocity and is related to the surface wind stress vector $\boldsymbol{\tau}$ by $\mathbf{u}_e = \boldsymbol{\tau} \times \mathbf{k}/(\rho_o f h_m)$, $w_e$ is the entrainment velocity, $T_d$ is the water temperature below the base of the mixed layer, and $\mathbf{u}_g$ is the surface geostrophic velocity and is related to the SSH by $\mathbf{u}_g = -g\nabla h \times \mathbf{k}/f$. In the following, we refer to the five terms in Eq. (2) as temperature tendency, surface heat flux forcing, Ekman advection, vertical entrainment, and geostrophic advection, respectively.

Instead of solving $T_m$ and $h_m$ prognostically using observed SSH, surface wind stress, and net surface heat flux data (Qiu and Kelly 1993), we analyzed the surface ocean heat budget in this study by using the $T_m$ and $h_m$ data from observations. Specifically, the $T_m$ field used is the monthly SST data of NCEP (Reynolds and Smith 1994), and the $h_m$ field is diagnosed from the monthly upper-ocean temperature data of the Joint Environmental Data Analysis (JEDA) Center of Scripps Institution of Oceanography (White 1995). Following Qiu and Kelly (1993), we defined the mixed layer as the surface ocean layer whose depth-averaged temperature is 1°C higher than the water temperature just below, that is,

$$\frac{1}{h_m}\int_{-h_m}^{0} T(z)\, dz - T_d \equiv 1^\circ\text{C}. \tag{3}$$

Thus defined, $T_m - T_d = 1.0$°C. In the Kuroshio Extension region of 31°–37°N, 141°E–180° the mean J/F/M mixed layer depth estimated from the JEDA data is about 210 m. For both the $Q_{\text{net}}$ and $\boldsymbol{\tau}$ fields, we used the monthly datasets from the NCEP reanalysis (Kalnay et al. 1996). Estimating $w_e$ in the vertical entrainment term in Eq. (2) commonly requires solving the turbulent kinetic energy equation in the mixed layer (e.g., Davis et al. 1981). Without solving this equation directly, we estimated $w_e$ again diagnostically in this study by using the $h_m$ field estimated from the JEDA dataset. Specifically,

$$w_e = \begin{cases} \Delta h_m/\Delta t, & \Delta h_m/\Delta t > 0 \\ 0, & \text{otherwise.} \end{cases} \tag{4}$$

To estimate each term in Eq. (2), we interpolated all variables onto a monthly 1° × 1° grid. Individual terms were then calculated and averaged in the Kuroshio Extension region and over the J/F/M period. Figures 8a–8d show the time series of the first four terms in Eq. (2) from 1982 to 1999 after removing their respective mean values (see Table 1). The linear correlation coefficient between the nonseasonal temperature tendency term (Fig. 8a) and the nonseasonal heat flux forcing term (Fig. 8b) is 0.47. This value of coefficient is similar to that found in the Kuroshio Extension region by Iwasaka and Wallace (1995), who used the Comprehensive Ocean–Atmosphere Data Set and compared these two terms in the North Pacific Ocean for the period of 1950–1979. Adding the contributions from the nonseasonal Ekman advection and vertical pumping terms better explains the nonseasonal temperature tendency time series. The linear correlation coefficient increases to 0.52 when both of these two terms are included (see Table 2). Despite this improvement, the correlation is still relatively low, suggesting the importance of heat advection by the ocean circulation in determining the nonseasonal $T_m$ changes. It is also worth emphasizing that the first four terms in Eq. (2) alone cannot close the *mean* surface ocean heat balance. As indicated in Table 1, the J/F/M mean value for temperature tendency in 1982–99 is $-2.63 \times 10^{-7}$ °C s$^{-1}$. In this same period, the mean value for the sum of surface heat flux forcing, Ekman advection, and vertical entrainment is $-3.89 \times 10^{-7}$ °C s$^{-1}$. The cooling is clearly overestimated if only the one-dimensional mixed layer processes are considered.

The SSH field measured by the T/P altimeters allows us to evaluate the geostrophic advective term for 1993–99. As shown in Fig. 8e, nonseasonal geostrophic advection, $-(\mathbf{u}_g \cdot \nabla T_m)'$, was negative in 1993–95 when the intensity of the Kuroshio Extension had a decreasing trend and positive in 1996–99 when this trend reversed. Notice that inclusion of geostrophic advection helps close the surface ocean heat balance both on the seasonal and interannual timescales. Seasonally, Table 1 shows that the warming effect due to geostrophic advection offsets the ''excessive'' cooling due to the combined surface heat flux forcing, Ekman advection, and vertical entrainment. For the period of 1993–99, inclusion of the geostrophic advection term reduces the surface ocean heat imbalance[1] to $0.18 \times 10^{-7}$ °C s$^{-1}$. For the nonseasonal $T_m$ signals in 1993–99, the linear correlation coefficient between the nonseasonal temperature tendency time series (Fig. 9a) and the time series of the sum of nonseasonal surface heat flux forcing, Ekman advection, and vertical entrainment (Fig. 9b) is only 0.38. Figure 9c shows the time series when the nonseasonal geostrophic advection term is added to the time series of Fig. 9b. The linear correlation coefficient in this case is 0.80. This increased correlation clearly demonstrates the importance of horizontal advection by the ocean circulation in influencing the nonseasonal wintertime SST changes in the Kuroshio Extension region. It is worth emphasizing that the $-(\mathbf{u}_g \cdot \nabla T_m)'$ term shown in Fig. 8e is largely determined by advection of mean temperature by the anomalous geostrophic flow $-(\mathbf{u}'_g \cdot \nabla \overline{T}_m)$. Advection of anomalous temperature by the mean geostrophic flow, $-(\overline{\mathbf{u}}_g \cdot \nabla T'_m)$, has little effect on the time series of $-(\mathbf{u}_g \cdot \nabla T_m)'$.

In concluding this section, we plot in Fig. 10 the linear

[1] This imbalance can be due to errors in estimating the individual terms in Eq. (2), and it can result from other effects, such as eddy diffusion and advection by ageostrophic flows, that have been neglected in Eq. (2).

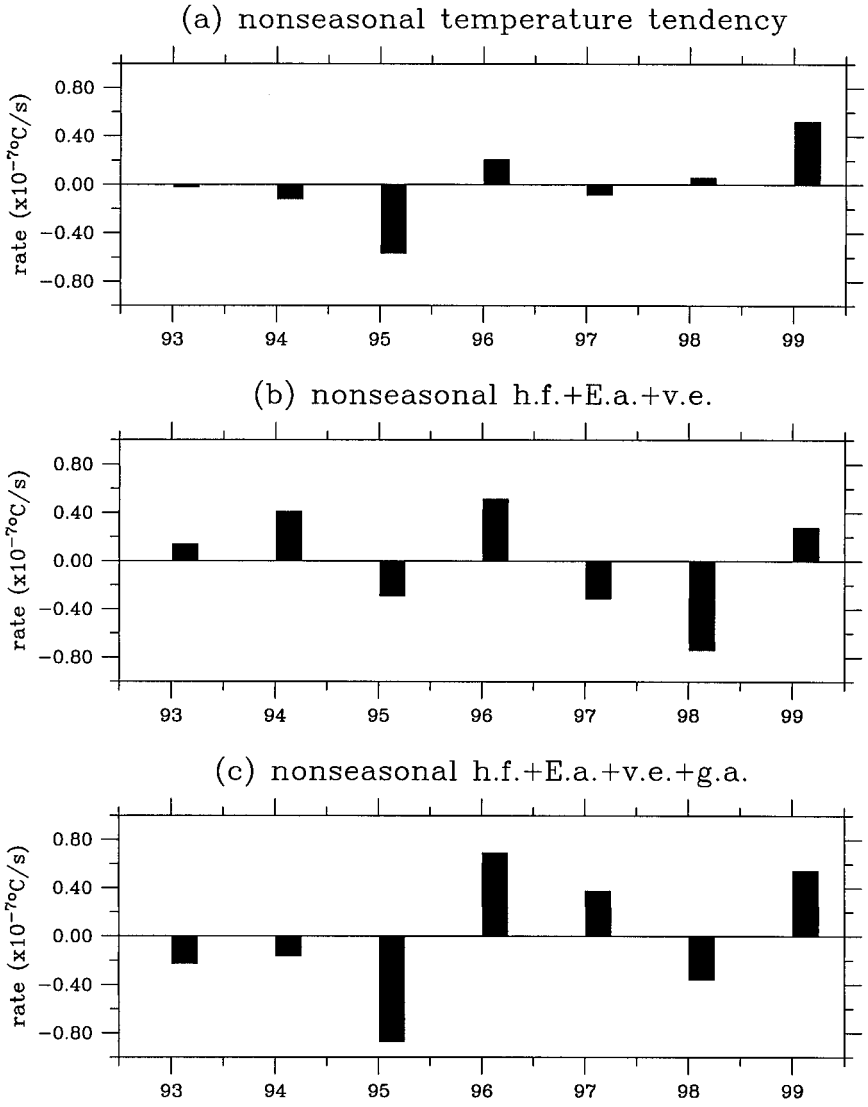


FIG. 9. Time series of the nonseasonal values for (a) temperature tendency; (b) sum of surface heat flux forcing, Ekman advection, and vertical entrainment; and (c) sum of surface heat flux forcing, Ekman advection, vertical entrainment, and geostrophic advection.

correlation coefficient between the time series of Fig. 7a and that of the wintertime SST anomalies at every 1° grid in the Pacific Ocean north of 10°S. The result shows the highest correlation, $r > 0.8$, exists in the Kuroshio Extension region downstream of the Shatsky Rise. In the upstream Kuroshio Extension region southeast of Japan, the correlation is not as high ($r \sim 0.6$–0.7). This is to be expected because mesoscale eddies and disturbances in the Kuroshio Extension system tend to move westward (e.g., Tai and White 1990; Qiu et al. 1991; Mitchell et al. 1996). With the presence of Japan and the Izu Ridge acting as a meridional barrier along 141°E, the westward-moving eddies and disturbances tend to accumulate in the upstream Kuroshio Extension region and induce local SST changes that are different from the SST changes associated with the large-scale Kuroshio Extension system. Figure 10 also shows that the interannual signals associated with the Kuroshio Extension system have only weak corresponding signals in the tropical Pacific Ocean. Since the interannual SST changes in the tropical Pacific Ocean are dominated by ENSO events, this suggests that the SST anomalies of the Kuroshio Extension shown in Fig. 7a are mostly independent of the ENSO-related tropical variability.

## 5. Summary

Long-term satellite altimeter observations over the past decade provide us now with a new means to investigate the interannual changes in the large-scale ocean circulation and their impact upon the upper ocean properties. Using the altimetric data from the T/P mis-

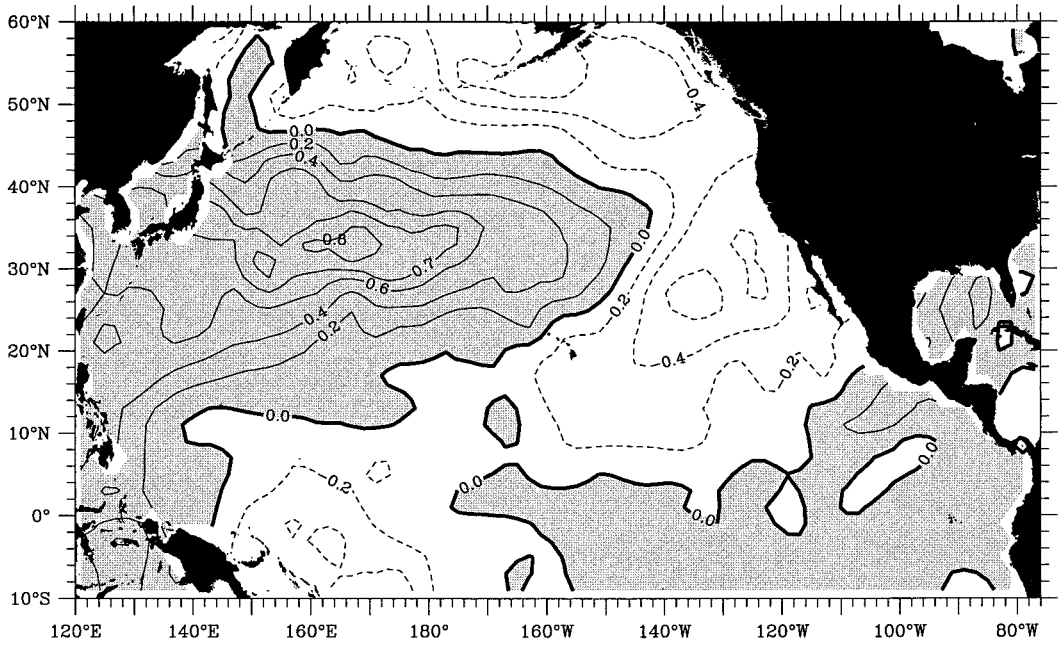


FIG. 10. Linear correlation coefficient between the wintertime SST anomaly time series of the Kuroshio Extension region (Fig. 7a) and the wintertime SST anomaly time series at each 1° grid of the equatorial and North Pacific Ocean. Contour intervals are 0.2 except for inclusion of the 0.7 contour. Shaded areas indicate positive correlation.

sion, we described in this study the large-scale, low-frequency changes in the Kuroshio Extension system and examined their impact on the wintertime SST anomaly field.

From October 1992 to 1996, the large-scale Kuroshio Extension system changed gradually from an elongated state to a contracted state. This interannual trend reversed in late 1997. In the elongated state, the Kuroshio Extension is characterized by its larger eastward surface transport and greater zonal penetration. Both of these characteristics are connected closely to the presence of an intense, zonally elongated southern recirculation gyre. During this elongated state, the zonal-mean Kuroshio Extension path is located at a more northerly latitude. In contrast, the Kuroshio Extension in the contracted state has a smaller eastward surface transport, a weaker southern recirculation gyre, and a more southerly mean path. Averaged zonally over the Kuroshio Extension system, the path migration fluctuated between 33.5° and 35°N and the sea surface height jump across the Kuroshio Extension changed from 0.45 to 0.7 m.

Over the T/P period, the mesoscale eddy field in the Kuroshio Extension region also underwent prominent interannual changes. In the upstream region west of the Shatsky Rise (141°–159°E), the eddy and mean kinetic energy levels varied out of phase, and the total kinetic energy level remained nearly constant. While the Kuroshio Extension was in the elongated state from 1992 to 1995, the mesoscale eddy activity was relatively weak and the high EKE band was confined narrowly along the Kuroshio Extension path. When the Kuroshio Extension was in the contracted state in 1996 and 1997, the EKE level in the upstream Kuroshio Extension region increased significantly. Downstream from the Shatsky Rise, the intensity of the mesoscale eddy field is controlled by the zonal penetration of the Kuroshio Extension jet: the EKE level is high when the Kuroshio Extension is in the elongated state and has a greater eastward zonal penetration.

An examination of the wintertime SST anomaly field in the Kuroshio Extension region reveals a well-defined interannual signal related to the interannual signal in the large-scale Kuroshio Extension system. Specifically, the warm (cold) wintertime SST anomalies tend to persist in years when the Kuroshio Extension system is in its elongated (contracted) state. Averaged in the Kuroshio Extension region, the SST anomalies have a peak-to-peak amplitude exceeding 1°C. To quantitatively assess the influence of the large-scale changes of the Kuroshio Extension on the wintertime SST distributions, we analyzed the surface ocean heat balance using the available SSH, upper ocean temperature, net surface heat flux, and surface wind stress data. The analysis shows that the heat advection by the Kuroshio Extension is not only important in closing the seasonal mean surface ocean heat balance, it also contributes significantly to the nonseasonal wintertime SST changes. In the seven winters (1993–99) for which the T/P data is available, we found that the nonseasonal geostrophic advection worked to reduce the nonseasonal wintertime SSTs when the Kuroshio Extension changed from the elongated state to the contracted state, whereas it worked to increase the

nonseasonal wintertime SSTs when the Kuroshio Extension shifted from the contracted state to the elongated state.

In this study, we have identified the large-scale, interannual changes of the Kuroshio Extension as migrations between an elongated and a contracted state and have emphasized the impact of these changes on the regional wintertime SST anomaly filed. The observed interannual changes in the Kuroshio Extension system can be regionally and/or remotely forced by surface wind and buoyancy forcings over the North Pacific Ocean. They can also result from the internal ocean dynamics associated with the southern recirculation gyre variability. Future studies are needed to clarify the cause and the dynamic/thermodynamic interplays of different physical processes.

*Acknowledgments.* This study benefited from many discussions with Drs. Kathie Kelly and Humio Mitsudera. Detailed comments made by the two anonymous reviewers helped clarify many parts of an early version of the manuscript. The SST, surface wind stress, and surface heat flux data were provided by the National Center for Environmental Prediction, the upper ocean temperature data by the Joint Environmental Data Analysis Center, and the TOPEX/Poseidon data by the Physical Oceanography DAAC at Jet Propulsion Laboratory. I am grateful to Dr. Gary Mitchum for his help in processing the original T/P data. Support from NASA through the Young Investigators Award (NAGW-5250) and the TOPEX/Poseidon Extended Mission project (Contract 960889) is gratefully acknowledged.

## REFERENCES

Adamec, D., 1998: Modulation of the seasonal signal of the Kuroshio Extension during 1994 from satellite data. *J. Geophys. Res.*, **103,** 10 209–10 222.

Barnett, T. P., D. W. Pierce, R. Saravanan, N. Schneider, D. Dommenget, and M. Latif, 1999: Origins of the midlatitude Pacific decadal variability. *Geophys. Res. Lett.*, **26,** 1453–1456.

Cayan, D. R., 1992: Latent and sensible heat flux anomalies over the Northern Oceans: Driving the sea surface temperature. *J. Phys. Oceanogr.*, **22,** 859–881.

da Silva, A. M., C. C. Young, and S. Levitus, 1994: *Atlas of Surface Marine Data 1994,* Vol. 1: *Algorithms and Procedures.* NOAA Atlas NESDIS 6, U.S. Dept. of Commerce, Washington, D.C., 83 pp.

Davis, R. E., R. de Szoeke, and P. Niiler, 1981: Variability in the upper ocean during MILE. Part II: Modeling the mixed layer response. *Deep-Sea Res.*, **28,** 1453–1475.

Deser, C., and M. L. Blackmon, 1995: On the relationship between tropical and North Pacific sea surface variations. *J. Climate,* **8,** 1677–1680.

——, M. A. Alexander, and M. S. Timlin, 1999: Evidence for a wind-driven intensification of the Kuroshio Current Extension from the 1970s to the 1980s. *J. Climate,* **12,** 1697–1706.

Gill, A., and P. P. Niiler, 1973: The theory of the seasonal variability in the ocean. *Deep-Sea Res.*, **20,** 141–177.

Hall, M. M., 1989: Velocity and transport structure of the Kuroshio Extension at 35°N, 152°E. *J. Geophys. Res.*, **94,** 14 445–14 459.

Huang, R. X., 1990: Does atmospheric cooling drive the Gulf Stream recirculation? *J. Phys. Oceanogr.*, **20,** 750–757.

Iwasaka, N., and J. M. Wallace, 1995: Large-scale air–sea interaction in the Northern Hemisphere from a view point of variations of surface heat flux by SVD analysis. *J. Meteor. Soc. Japan,* **73,** 781–794.

Kalnay, E., and Coauthors, 1996: The NCEP/NCAR 40-Year Reanalysis Project. *Bull. Amer. Meteor. Soc.,* **77,** 437–471.

Kawai, H., 1972: Hydrography of the Kuroshio Extension. *Kuroshio—Its Physical Aspects,* H. Stommel and K. Yoshida, Eds., University of Tokyo Press, 235–354.

Kelly, K. A., 1991: The meandering Gulf Stream as seen by the Geosat altimeter: Surface transport, position, and velocity variance from 73° to 46°W. *J. Geophys. Res.*, **96,** 16 721–16 738.

——, and S. T. Gille, 1990: Gulf Stream surface transport and statistics at 69°W from the Geosat altimeter. *J. Geophys. Res.*, **95,** 3149–3161.

——, S. Singh, and R. X. Huang, 1999: Seasonal variations of sea surface height in the Gulf Stream region. *J. Phys. Oceanogr.*, **29,** 313–327.

Latif, M., and T. P. Barnett, 1994: Causes of decadal climate variability over the North Pacific and North America. *Science,* **266,** 634–637.

——, and ——, 1996: Decadal climate variability over the North Pacific and North America: Dynamics and predictability. *J. Climate,* **9,** 2407–2423.

Levitus, S., 1982: *Climatological Atlas of the World Ocean.* NOAA Prof. Paper No. 13, U.S. Govt. Printing Office, Washington, D.C., 173 pp.

Miller, A. J., D. R. Cayan, T. P. Barnett, N. E. Graham, and J. M. Oberhuber, 1994: Interdecadal variability of the Pacific Ocean: Model response to observed heat flux and wind stress anomalies. *Climate Dyn.,* **9,** 287–302.

——, ——, and W. B. White, 1998: A westward-intensified decadal change in the North Pacific thermocline and gyre-scale circulation. *J. Climate,* **11,** 3112–3127.

Mitchell, J. L., W. J. Teague, G. A. Jacobs, and H. E. Hurlburt, 1996: Kuroshio Extension dynamics from satellite altimetry and a model simulation. *J. Geophys. Res.*, **101,** 1045–1058.

Mizuno, K., and W. B. White, 1983: Annual and interannual variability in the Kuroshio current system. *J. Phys. Oceanogr.,* **13,** 1847–1867.

Nakamura, H., G. Lin, and T. Yamagata, 1997: Decadal climate variability in the North Pacific during the recent decades. *Bull. Amer. Meteor. Soc.,* **78,** 2215–2225.

Peng, S., W. A. Robinson, and M. P. Hoerling, 1997: The modeled atmospheric response to midlatitude SST anomalies and its dependence on background circulation states. *J. Climate,* **10,** 971–987.

Qiu, B., 1995: Variability and energetics of the Kuroshio Extension and its recirculation gyre from the first two-year TOPEX data. *J. Phys. Oceanogr.,* **25,** 1827–1842.

——, and K. A. Kelly, 1993: Upper ocean heat balance in the Kuroshio Extension region. *J. Phys. Oceanogr.,* **23,** 2027–2041.

——, ——, and T. M. Joyce, 1991: Mean flow and variability in the Kuroshio Extension from Geosat altimetry data. *J. Geophys. Res.,* **96,** 18 491–18 507.

Reynolds, R. W., and T. M. Smith, 1994: Improved global sea surface temperature analyses using optimum interpolation. *J. Climate,* **7,** 929–948.

Schmitz, W. J., Jr., 1984: Observations of the vertical structure of the eddy field in the Kuroshio Extension. *J. Geophys. Res.*, **89,** 6355–6364.

Stammer, D., 1997: Steric and wind-induced changes in TOPEX/POSEIDON large-scale sea surface topography observations. *J. Geophys. Res.*, **102,** 20 987–21 009.

Tai, C.-T., and W. B. White, 1990: Eddy variability in the Kuroshio Extension as revealed by Geosat altimetry: Energy propagation away from the jet, Reynolds stress, and seasonal cycle. *J. Phys. Oceanogr.,* **20,** 1761–1777.

Vivier, F., K. A. Kelly, and L. Thompson, 1999: The contributions of wind forcing, waves, and surface heating to sea surface height

observations in the Pacific Ocean. *J. Geophys. Res.*, **104,** 20 767–20 788.

Wang, L., and C. J. Koblinsky, 1996: Annual variability of the subtropical recirculations in the North Atlantic and North Pacific: A TOPEX/Poseidon study. *J. Phys. Oceanogr.*, **26,** 2462–2479.

——, ——, and S. Howden, 1998: Annual and intraannual sea level variability in the region of the Kuroshio Extension from TOPEX/Poseidon and Geosat altimetry. *J. Phys. Oceanogr.*, **28,** 692–711.

White, W. B., 1995: Design of a global observing system for gyre-scale upper ocean temperature variability. *Progress in Oceanography*, Vol. 36, Pergamon, 169–217.

Wyrtki, K., L. Magaard, and J. Hagar, 1976: Eddy energy in the oceans. *J. Geophys. Res.*, **81,** 2641–2646.

Xie, S.-P., T. Kunitani, A. Kubokawa, M. Nonaka, and S. Hosoda, 2000: Interdecadal thermocline variability in the North Pacific for 1958–97: A GCM simulation. *J. Phys. Oceanogr.*, in press.

Yamagata, T., Y. Shibao, and S.-I. Umatani, 1985: Interannual variability of the Kuroshio Extension and its relation to the Southern Oscillation/El Niño. *J. Oceanogr. Soc. Japan*, **41,** 274–281.

Yasuda, I., K. Okuda, and M. Hirai, 1992: Evolution of a Kuroshio warm-core ring—Variability of the hydrographic structure. *Deep-Sea Res.*, **39,** 131–161.